Humidity tolerant ultra-thin NiO gas sensing films

Rachel L. Wilson[1], Cristian Eugen Simion[2], Adelina Stanoiu[2], Alaric Taylor[3], Stefan Guldin[3], James A. Covington[4], Claire J. Carmalt[1] and Chris S. Blackman[1,*]

[1] Christopher Ingold Laboratories, Department of Chemistry, University College London, 20 Gordon Street, London WC1H 0AJ, United Kingdom.
[2] National Institute of Materials Physics, Atomistilor 405A, 077125, Magurele, Romania
[3] Department of Chemical Engineering, University College London, Torrington Place, London, WC1E 7JE
[4] School of Engineering, University of Warwick, Coventry CV4 7AL, UK

**Corresponding author; c.blackman@ucl.ac.uk*

Abstract

When the gas sensor active layer film thickness is decreased increased sensitivity to changes in the adsorbate concentration are expected when measuring the resistance of the layer, in particular when this thickness is on the order of the Debye length of the material (one to tens of nanometers), however this is demonstrated only for a limited number of materials. Herein, ultra-thin NiO films of different thickness (8 to 21 nm) have been deposited *via* chemical vapour deposition to fabricate gas sensor devices. Sensor performance toward a range of NO_2 concentration (800 part-per-billion to 7 part-per-million) was evaluated and an optimum operating temperature of 125°C determined. The dependence of the potential relative changes with respect to the NO_2 concentration and of the sensor signal with respect to the geometrical parameters were qualitatively evaluated in order to derive a transduction model capable to fit the experimental results. The selective sensitivity towards NO_2 was confirmed by the limited response for different reducing gases, CO, CH_4, NH_3 and SO_2 under optimum operating conditions, and the sensor signal towards NO_2 increased with decreasing thickness, demonstrating that the concept of a Debye length dependence of sensitivity is applicable for the *p*-type semiconductor NiO. In addition, these NiO sensors were exposed to different relative levels of humidity over a wide range of operating temperatures and found to display humidity tolerance far superior to previous reports for SnO_2 materials.

Key words: nickel oxide, thickness dependence, humidity, NO_2 sensing, low temperature

Semiconducting metal oxide based sensors (MOS) are ubiquitous in the gas sensor market for detecting hazardous gases [1], with *n*-type SnO_2 and WO_3 being the most commercially successful sensing materials. In contrast, *p*-type MOS based sensors such as CuO, NiO and Co_3O_4 have received much less attention [2]. Over the last ten years out of more than 8000 total articles on MOS, only 14% were on *p*-type metal oxides. One reason for the lack of attention may be linked to the fact that *p*-type materials typically exhibit lower sensitivity in comparison with *n*-type MOS [3]. However, *p*-type materials offer several interesting material characteristics for developing new sensing functionalities, for instance some *p*-type materials have been found to be tolerant to interference from humidity, which can be a major issue with their *n*-type counterparts that limits their use in real-world applications [4]. For instance when considering the activation energy of conductance of granular tin dioxide pellets McAleer et al found that on heating from room temperature to approximately 280 deg. C in dry air that a linear change in resistance was observed with activation of conductance of approximately 0.28 eV, very close to the value associated with donor defects in SnO_2 [5]. However on varying the humidity of the air they found that whilst the activation energy of conductance of SnO_2 pellets did not vary, the measured resistance increased approximately thirty times on going from humid to dry air, i.e. water was acting as a surface donor state. Thus it can be inferred that whilst the overall resistance in their *n*-type SnO_2 samples was dominated by bulk donor defects, water had a strong effect on the overall resistance. One promising candidate *p*-type sensing material, NiO, which behaves as a *p*-type semiconductor due to the presence of nickel defects within the material even at moderate temperatures (above 150 K) [6], has complex and variable oxygen desorption [7,8], which due to the importance of surface oxygen species in mediating gas sensing reactions could lead to an evolution of temperature-dependent specific analyte interactions, and hence selective response. Due to these interesting material characteristics we were interested in exploring *p*-type semiconducting metal oxides, and in particular NiO, for selective and humidity tolerant gas sensing.

Most current published papers on gas sensing properties of NiO omit the evaluation of the gas sensing performances under ‘in-field’ conditions, i.e. the presence of moisture at normal atmospheric pressure and different interfering agents [9]. Operation at variable humidity is particularly relevant for NiO, given that NiO has a high affinity towards hydroxyl species and the

previous reports of moisture significantly increasing its sensitivity towards low concentrations of NO_2 [10,11].

When film thickness is decreased in a monolithic layer of an *n*-type semiconductor, the oxygen adsorbate-induced electron-depleted layer makes up a greater proportion of the material, providing increasing sensitivity to changes in the adsorbate concentration when measuring the resistance of the layer [12]. Du *et al* reported the use of atomic layer deposition (ALD) for exploring the effect of film thickness on the gas sensor response of *n*-type SnO_2. [13]. An optimum sensitivity towards CO was found for a film thickness of 3 nm, which was correlated with the Debye length for SnO_2. In our own work [14] we also demonstrated the sensitivity dependence of ultra-thin TiO_2 films with respect to film thickness on the order of nanometres. For the case of *p*-type MOS the enhancement of sensitivity on reduction of film thickness may be less pronounced, due to the electrode-semiconductor dead contact and the highly resistive gas insensitive core, which are expected to have dominant roles in the measurement of electrical resistance [15]. Indeed, in one of the few papers describing the gas sensing and transducing principles for *p*-type materials it was found that for granular materials the morphological aspects (involving the grain size with respect to the Debye length) need to be considered when evaluating the gas sensing performances [16]. We have recently developed a chemical vapor deposition (CVD) route to ultra-thin films, enabling fine control over the resulting film thickness down to the nanometer level [17], and herein, we report on a systematic evaluation of the gas sensing capabilities of NiO as a function of film thickness and ambient humidity, with the aim of evaluating sensitivity and humidity tolerance.

Experimental

Thin Film Synthesis

CVD of nickel oxide thin films were performed using a flow-type, cold-walled reactor described previously [14]. The reactor was programmed using a custom IGI Systems Lab Interface Input control box, which automatically controls all temperatures and heating systems, gas flow rates and solenoid valves. CVD experiments were carried out using $[Ni(dmamp')_2]$, (dmamp' = 2-dimethylamino-2-methyl-1-propanolate) [17]. Pure shield argon gas (99.998%) supplied by British Oxygen Company (BOC), was used as the carrier gas for all depositions. Gas flow rates were controlled using Mass Flow Controllers (MFC's) purchased from Brooks Instrument (GF40

model number), with flow rates varying from 20 - 700 sccm. The reactor running pressures therefore varied in the range of ~ 1.0 - 7.0 mbar. Single-sided alumina sensor platforms, in which the heater track and sensor electrodes are separated by an insulating glassy ceramic, were used as obtained [14] (University of Warwick), and microscope slides (super premium, VWR) were cleaned using iso-propanol (Sigma Aldrich, 99.5%) and air dried before loading into the reactor. Whilst the substrate holder was being heated to the required temperature (250 - 400°C), the reactor was pumped down under vacuum to achieve a base pressure of ~ 4 x 10^{-2} mbar. Gas flows were then turned on, where the running pressure was recorded. [Ni(dmamp')$_2$] was introduced into the reaction chamber by passing the carrier gas into the bubbler to assist the transportation of vaporized precursor molecules. To prevent the precursor condensing or reacting in the pipework, the bubbler outlet line was held at a temperature higher than the bubbler temperature but lower than the substrate temperature. Films were deposited by continuously dosing the metal precursor from a bubbler held at 80 ºC under a flow rate of 20 sccm into the reactor under a constant flow of argon gas (20 sccm) at the given temperature until the desired reaction time/film thickness had been reached.

Atomic Force Microscopy (AFM)

AFM measurements were obtained using a Nanosurf Easy Scan Atomic Force Microscope, with a 10 μm Bruker NCLR tip in non-contact tapping mode. Scan areas were 5 x 5 μm, with measurements recorded at 250 points/line (20 nm lateral resolution) with 1 sec/line scan time. Data recorded were the arithmetic average roughness (Ra) and the root mean square roughness (Rq or RMS).

X-Ray Diffraction (XRD)

XRD measurements were performed using a Bruker-Axs D8 (GADDS) diffractometer, which operates with a Cu X-ray source, monochromated ($K_{\alpha1}$ and $K_{\alpha2}$) and a 2D area X-ray detector with a resolution of 0.01°. The diffraction patterns obtained were compared with database standards from the Inorganic Crystal Structure Database (ICSD), Karlsruhe, Germany. The beam spot is approximately 5 mm^2, which means that several areas of the sample can be analysed separately. For all thin films analysed an incident angle of 0.5 - 1° was used, and the diffracted X-rays were detected at angles from 10 - 66°.

X-Ray Photoelectron Spectroscopy (XPS)

XPS analysis was performed using a Thermo Scientific K-Alpha X-ray photoelectron spectrometer with monochromated Al K-alpha radiation, a dual beam charge compensation system and constant pass energy of 50 eV. Survey scans were collected in the range 0 - 1200 eV. XPS data was fitted using CasaXPS software. The principal peaks of interest were Ni 2p O 1s, Si 2p and C 1s. The escape depth in this system was in the range of 1-10 nm. Depth profiling was carried out via argon ion sputtering.

Gas sensing investigations

The gas sensing investigations were carried out using a computer control gas mixing system (GMS), equipped with 11 gas channels. Each channel is comprised of a mass flow controller (MFC, Bronkhorst) and two solenoid valves, with the MFC connected to high-grade certified gas which is subsequently diluted with dry or humid air (as carrier gas) to the desired target gas concentration. To generate humid air, the dry synthetic air carrier gas is passed through a water trap to saturate the atmosphere, and subsequently diluted with dry air in order to adjust the relative humidity (RH) ratio in the range between 0 to 90%. The total flow was kept constant during the measurements at 200 sccm. Each sensor was attached to a TO-5 socket electrically connected to a power supply (providing the necessary voltage to the heater meander) and to a scanner card of a Keithley 6517A able to acquire the electrical signals variations from the sensitive layers (see Figure 1), and placed into a PTFE chamber.

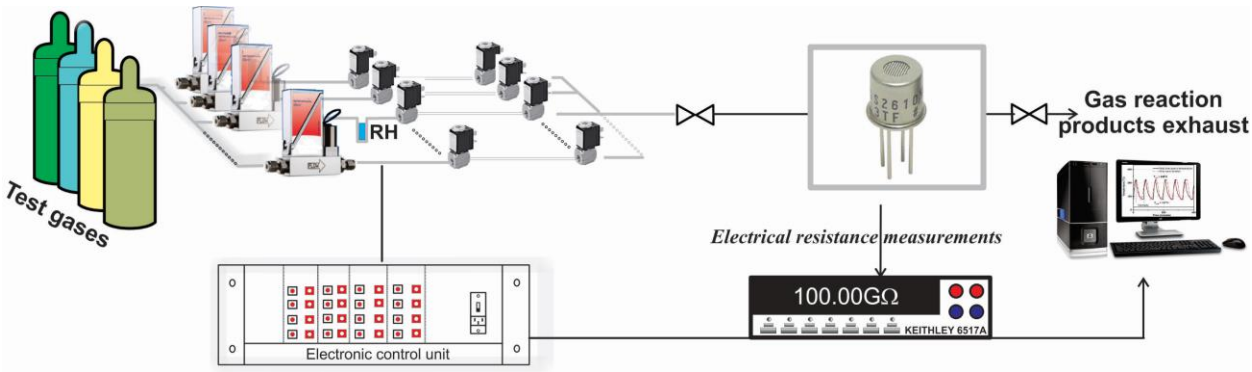

Fig. 1. Schematic representation of the experimental set-up used to evaluate the sensing performances of NiO sensitive materials.

Dedicated software (Agilent) is used to control the GMS and the electrical acquisition data devices via PC-GPIB interfaces. All sensors were subject to heater calibration as function of applied voltage by using a digital pyrometer (LumaSense IN 5-L Plus). The spot size for acquiring IR radiation was set to 2 mm^2 in order to cover most of the sensitive surface of the sensitive layer (Figure 2).

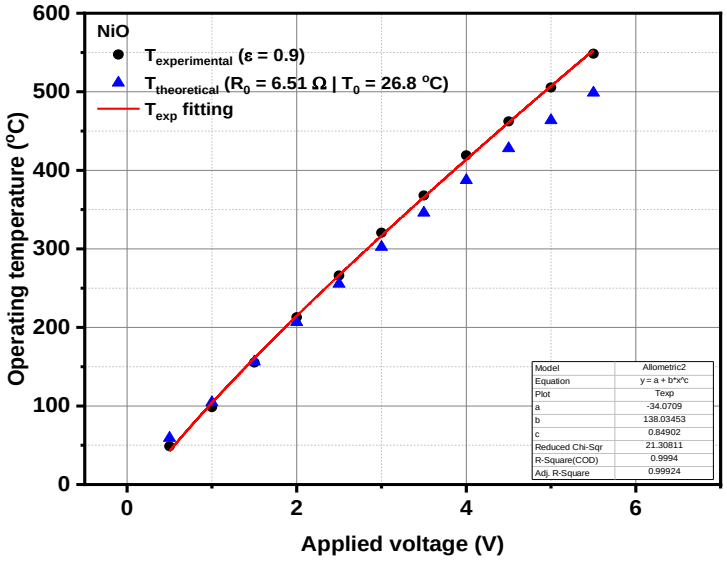

Fig. 2. Operating temperature as a function of the applied voltage to the heater

Spectroscopic ellipsometry

Optical measurements were carried out on a Semilab SE-2000 ellipsometer in a wavelength range from 250 to 990 nm and at angles of incidence varying from 60 to 75°. Microspot optics served to focus the beam spot size to 3.5 mm in the minor axis. The Semilab Spectroscopic Ellipsometry Analysis (SEA) software was used for fitting of the experimental data to an optical model. The NiO film were constructed with two components, a Tauc-Lorentz and a Cauchy dispersion function. An air-NiO diffusion layer *via* a Bruggerman effective medium approximation was further incorporated in order to account for surface roughness of the films.

Results and Discussion

Film Deposition

Figure 3 presents the X-ray diffraction (XRD) measurements for films deposited at different temperatures.

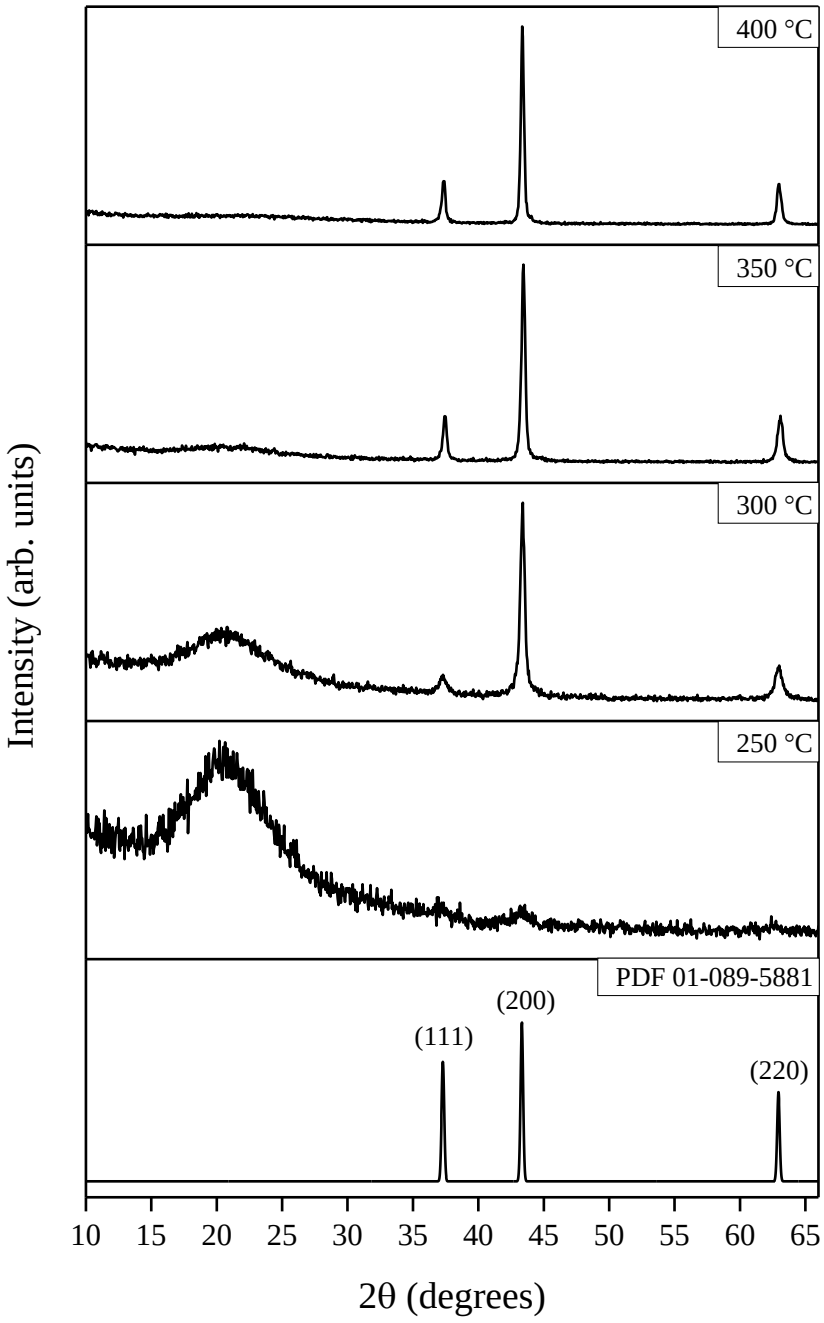

Fig. 3. Typical XRD patterns for NiO films deposited by CVD of [Ni(dmamp)$_2$] at various temperatures. Typical NiO reference pattern included [PDF 01-089-5881]

The XRD patterns show that films deposited at 250°C (~ 23 nm) were weakly diffracting, with the NiO (200) peak only just visible. This is likely due to the films being too thin to produce significant diffraction, which is consistent with the appearance of a broad background peak attributed to the

underlying amorphous glass substrate. For films deposited at 300 °C and above, NiO peaks become visible, with the (200) reflection the most intense (NiO PDF reference number 01-089-5881). As the growth temperature increased, so did the intensity of the NiO peaks increased, with the relative peak intensity ratio between the (111), (200) and (220) reflections becoming smaller. It was noted that the recorded peak intensities do not match those of the reference pattern, which suggests a preferred orientation of growth along the [100] direction.

The surface morphology of the NiO films was studied using non-contact mode atomic force microscopy (AFM). The AFM images presented in Figure 4 show that as the growth temperature increased, the surface roughness of the NiO films also became more pronounced.

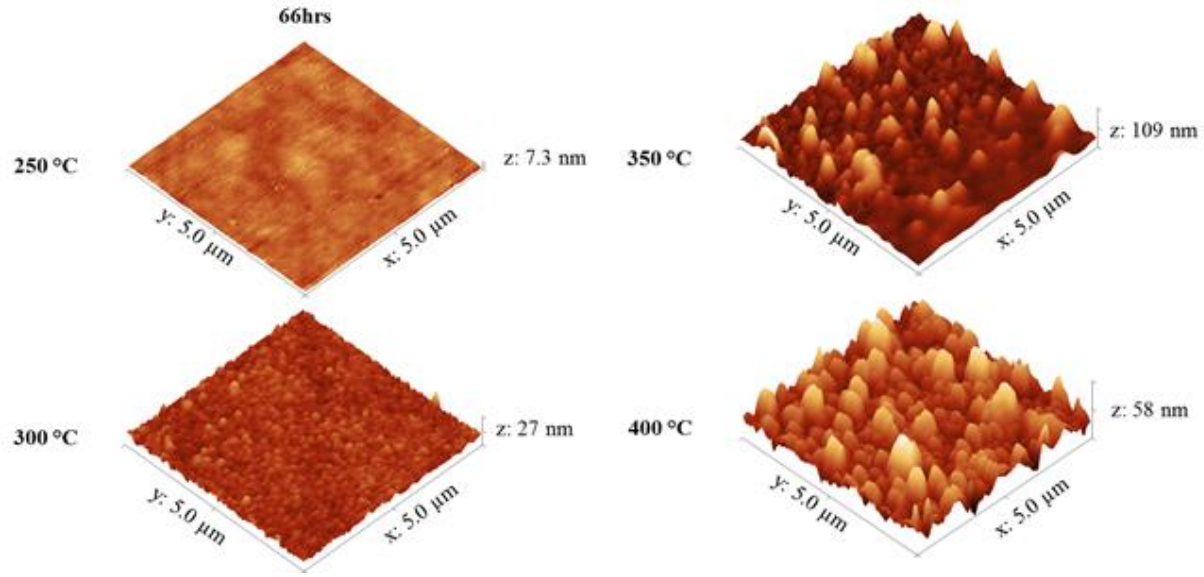

Fig. 4. AFM images of NiO films deposited by CVD of [Ni(dmamp)$_2$] at different substrate temperatures.

To determine the elemental composition and electronic state of the elements within the NiO films, X-ray photoelectron spectroscopy (XPS) was performed.

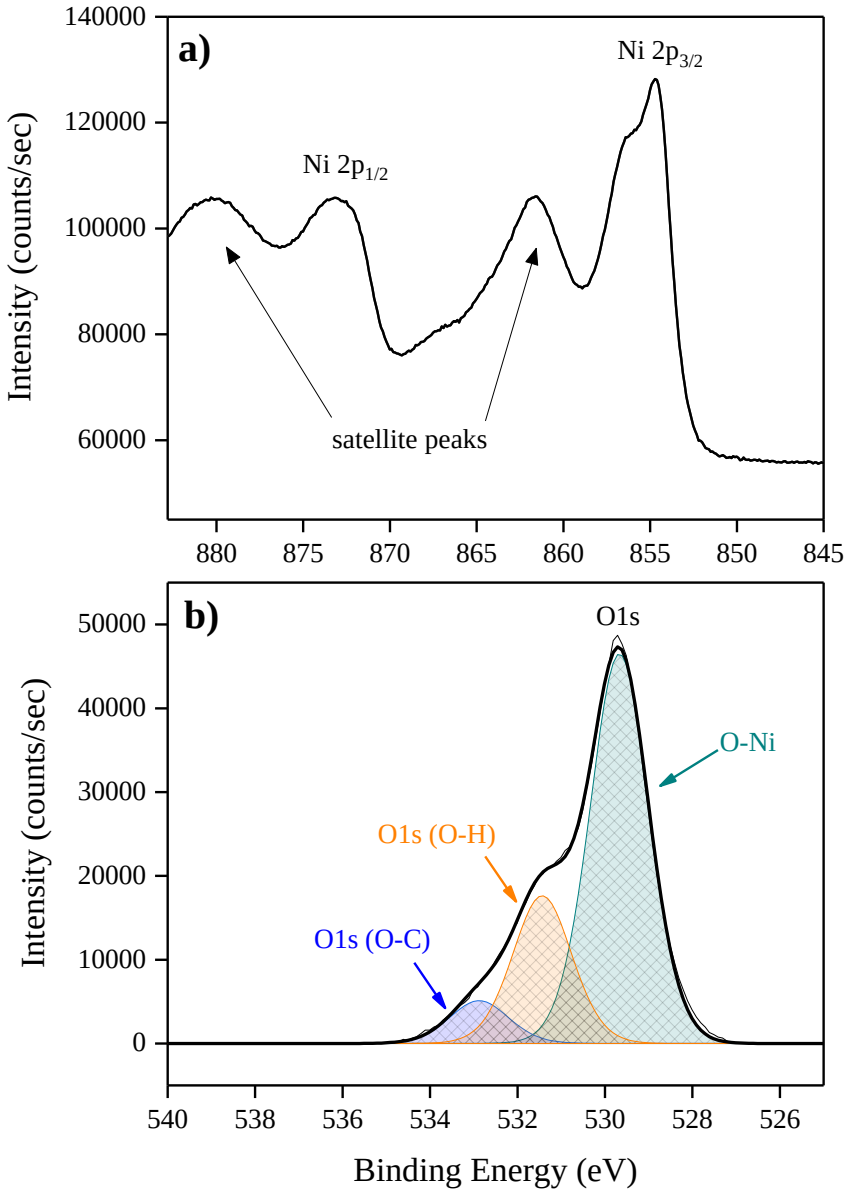

Fig. 5. Representative high resolution surface XPS spectra of a) Ni2p peak and b) de-convoluted O1s peak for NiO films. Peaks fitted with FWHM value of 1.6 eV

The data for a film deposited at 300°C, reveals the presence of Ni and O elements on the film surface with minimal contaminants present. High resolution surface scans (Figure 5a) of the Ni 2p peak confirm the presence of Ni^{2+}, with $2p_{3/2}$ and $2p_{1/2}$ peak binding energies of 855.4 eV and 873.2 eV respectively, with a peak separation of 17.8 eV. These values are within ± 0.2 eV of literature values [18,19]. Characteristic satellite peaks for the $2p_{3/2}$ and $2p_{1/2}$ peaks were observed

at 861.8 ± 0.2 eV and 880.2 ± 0.2 eV respectively. The prominent satellite shoulder 1.8 eV above the Ni $2p_{3/2}$ principal peak is unique to NiO [20]. De-convolution of the O 1s peak reveals three peaks. The two peaks at higher binding energy, 532.8 ± 0.2 eV and 531.4 ± 0.2 eV can be attributed to surface bound carbon and surface adsorbed water, respectively. The peak with the lowest binding energy (529.6 ± 0.2 eV) is attributed to the O 1s core peak of O^{2-} bound to Ni^{2+} (Figure 5b). Again, these peaks are consistent with literature values.

Since 300°C provided films with appreciable crystallinity and uniform crystallites, the relationship between deposition time at 300°C and NiO film thickness was investigated in order to identify conditions for growth of ultra-thin NiO films for use in gas sensing devices. Figure 6 shows that as the CVD deposition time was reduced to below 12 hours, the relationship between deposition time and film thickness altered from the growth rate found for longer deposition times. An initial nucleation period is commonly observed during CVD, during which the growth rate differs from the steady-state deposition rate.

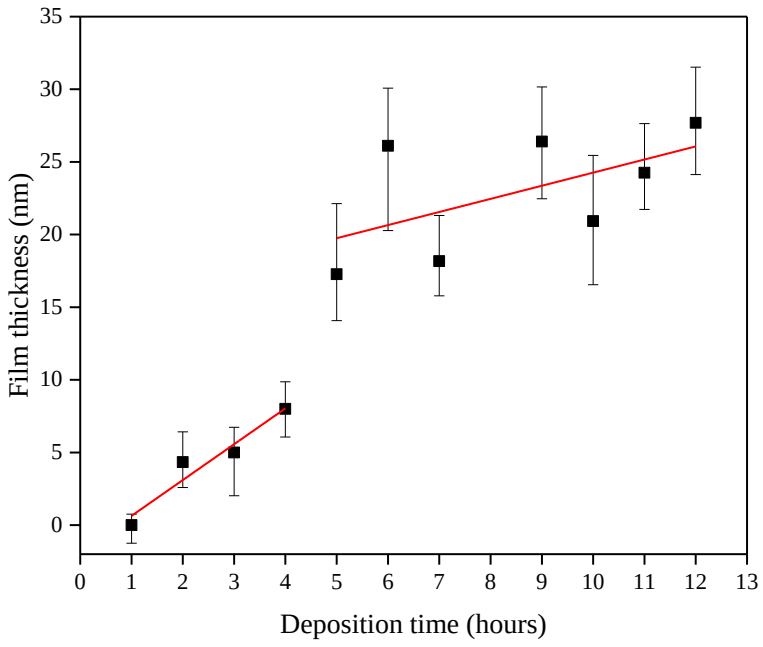

Fig. 6. Relationship between deposition time and film thickness for ultra-thin NiO films deposited by CVD of $[Ni(dmamp)_2]$ at a growth temperature of 300°C

Utilization of the Scherrer equation allowed an approximate calculation of the mean crystallite size for these NiO films, [21] by measuring the broadening of the X-ray reflections from the (200) crystallographic plane. For an NiO film of around 5 nm in thickness, Scherrer analysis indicated approximately 7 nm crystallites (in the [200] direction). As the film thickness increased (from 5 up to 50 nm) the approximate crystallite size also increases (from 7 up to 17 nm) with an increase in the approximate number of crystallite layers increasing too (from 1 to 3).

Gas sensing results

It is generally accepted that ambient moisture is the main interfering agent for infield applications of chemoresistive sensors. It has been suggested that *p*-type materials may be more humidity tolerant than *n*-type materials although with limited experimental evidence [22]. Accordingly, our NiO sensors were exposed to different relative humidity (RH) levels over a wide range of operating temperatures (Figure 7a-d).

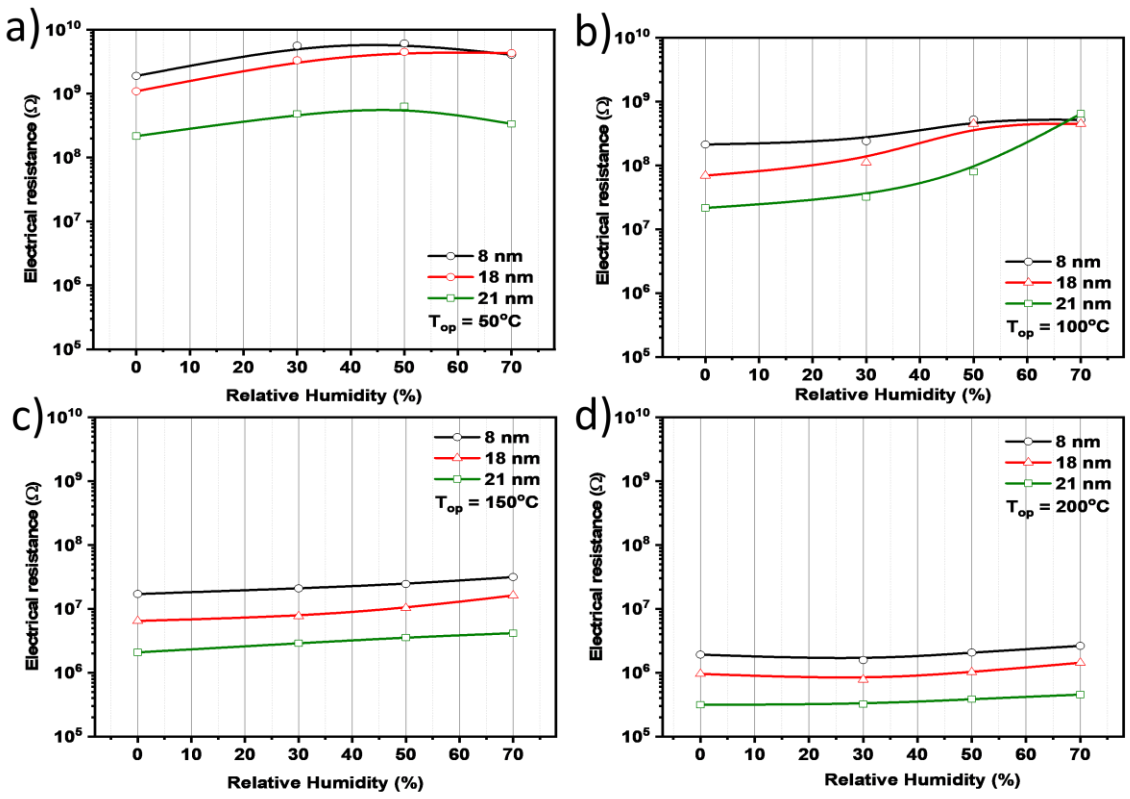

Fig. 7. The electrical resistance dependence with respect to the relative humidity for different thicknesses of NiO sensors operated at 50°C (a), 100°C (b), 150°C (c) and 200°C (d).

The electrical resistance decreased monotonously by 4 to 5 orders of magnitude with the increase in the operating temperature from 50°C to 200°C, as expected for a semiconductor. Varying RH in the range 0% to 70% at a given temperature (Figure 7) altered the measured resistance of our NiO films by only a factor of three (except for the 21 nm thick sample at 100°C where this variance limit was only maintained up to 50% RH). Similar results have been observed previously in literature (Supporting Information). In contrast for pellets of *n*-type SnO_2 the measured resistance increased approximately thirty times on going from humid (50% RH) to dry air [5]. In other words, *p*-type NiO is significantly more tolerant to humidity than *n*-type SnO_2.

The activation energies of conduction were obtained using the Arrhenius equation: $R = K * exp\left({}^{-E_a}/_{k_B T}\right)$, where R is the electrical resistance of the sensitive material, K is a constant, E_a is the activation energy, k_B is the Boltzmann constant and T is the absolute temperature. The plot of the activation energies with respect to the RH background is shown in Figure 8.

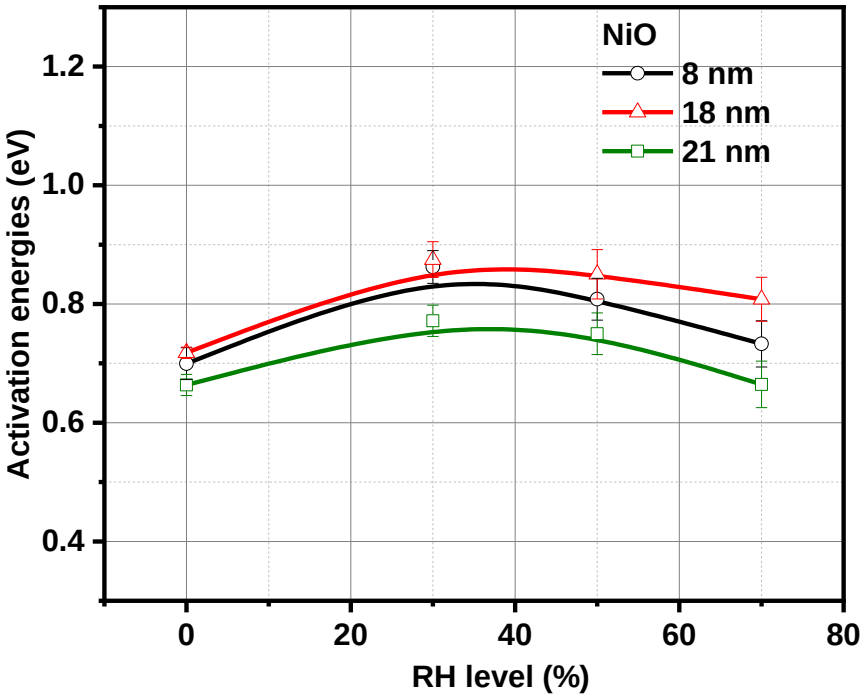

Fig. 8. The activation energies dependence for NiO sensors with respect to the RH level computed based on the results presented in Fig. 7.

The E_a for NiO sensors exhibited a scattering around the value of 0.8±0.1eV irrespective of the relative humidity, which matches that of experimentally determined acceptor defects in NiO [23, 24], and is within the range of values (0.4 – 0.8 eV) found for NiO films deposited using magnetron sputtering [25]. It may therefore be inferred that the conductance of NiO is dominated by bulk acceptor defects in this temperature range and that humidity does not alter the dominant conduction mechanism.

Nitrogen dioxide (NO_2) is a strong oxidizing gas and is considered to form a surface acceptor state on metal oxides; in the case of *p*-type MOS materials trapping of electrons from the valence band by a surface acceptor state is expected to lead to an increase in the hole concentration near the surface enhancing the overall conduction. When exposed to 3 parts-per-million (ppm) NO_2 (the EU mandated limit) the maximum peak in sensitivity was found at an operation temperature of 125 °C for a NiO film thickness of 8 nm (see Figure 9). Similar behavior was obtained for the other NiO sensors (18 and 21 nm).

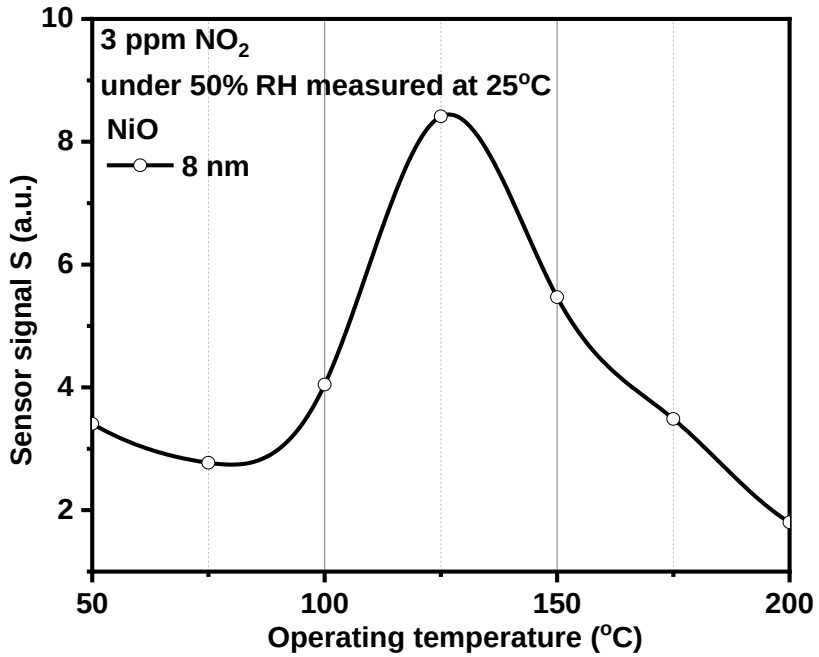

Fig. 9. Sensor signal for 3 ppm NO_2 exposure under 50% RH with respect to the operating temperature.

At this optimum operating temperature, the sensor signal was acquired over a wide range of NO_2 concentration (800 ppb to 7 ppm), in general exceeding the performance for thicker NiO film sensors reported elsewhere (Supporting Information). As seen in Figure 10 the magnitude of the sensor signal depended on the film thicknesses. As the film thickness decreased, the sensor signal increased under the same operating conditions.

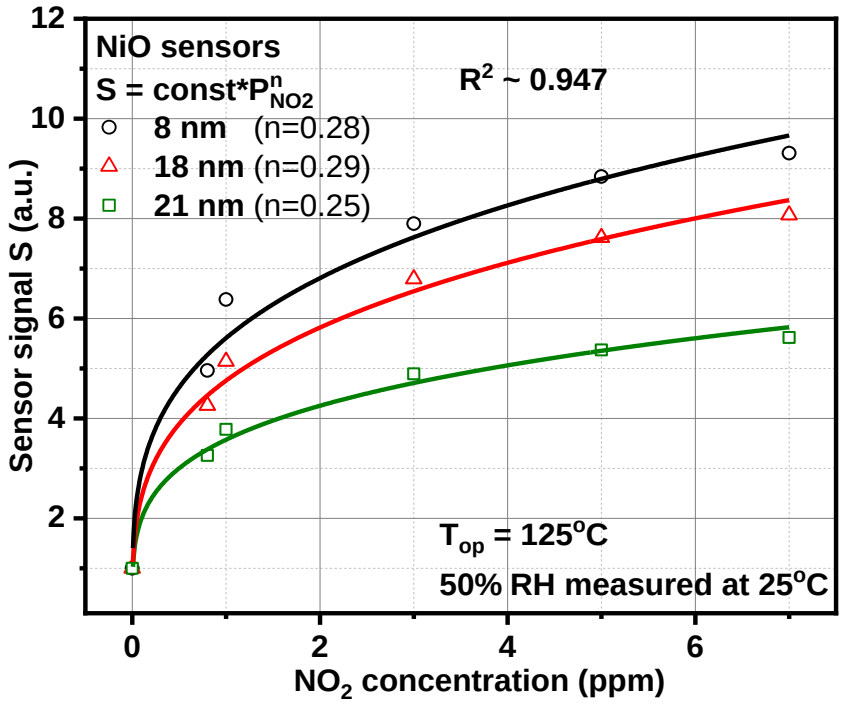

Fig. 10. Sensor signal dependence with respect to the NO_2 concentration for different NiO film thicknesses, when operated at 125°C.

All the sensors obeyed a power law dependence, namely:

$$S = const * p_{NO2}^{n} \quad (1)$$

where n represents the power law exponent with respect to the NO_2 concentration [26, 27], consistent with the description given by Barsan et al. [15].

In order to derive a transduction model that fits the experimental results, one has to obtain the dependence of the potential changes ($q\Delta V_s$) with respect to the NO_2 concentration and also the dependence of the sensor signal with respect to the layer thickness. We have qualitatively evaluated the relative changes in barrier potential with respect to the NO_2 concentration (see Figure

11). The experimental data were fitted using a power law dependence providing the energy value (0.001 eV) of the initial band bending (qV_{air}) prior to NO_2 exposure. Upon NO_2 exposure the conduction and valence bands bent upwards up to a level determined by the relation [28]:

$$qDV_s = 2k_BT \ln S \quad (2)$$

were $q\Delta Vs$ is the relative band bending upon NO_2 exposure; k_BT = 0.034 eV is the thermal energy at 125°C, and S represents the average of the sensor signals presented in Figure 10;

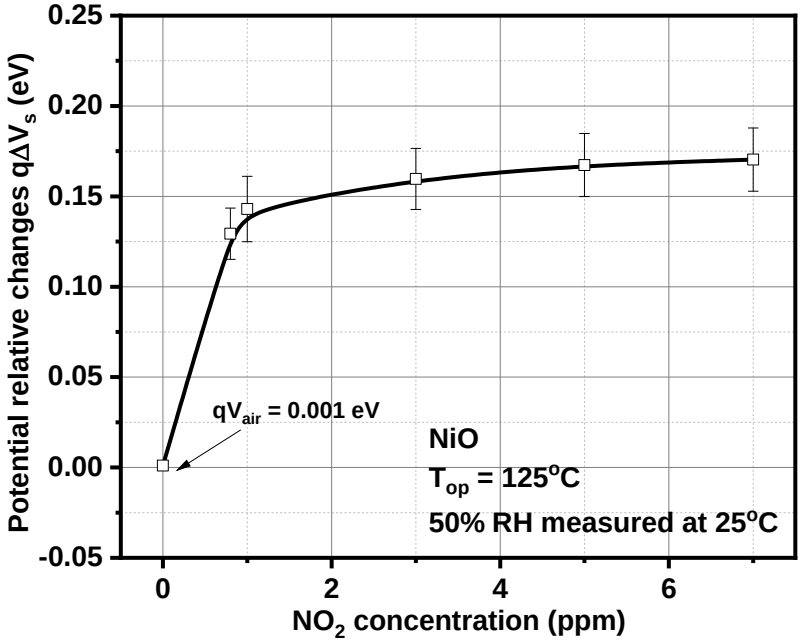

Fig. 11. The dependence of the potential relative changes ($q\Delta V_s$) with respect to the NO_2 concentration.

In order to get insights about the way in which the film thickness influences the overall sensitivity, we use equation (3) to derive the theoretical dependence and the subsequent fitting function (see Figure 12).

$$S = \frac{R_{air}}{R_{gas}} = \frac{\frac{L_d}{g}\cdot exp\left(\frac{-qV_{air}}{2*k_BT}\right)+\frac{1}{1+\frac{L_d}{d}\cdot exp\left(\frac{qV_{air}}{2*k_BT}\right)}}{\frac{L_d}{g}\cdot exp\left(-\frac{qVgas}{2*k_BT}\right)+\frac{1}{1+\frac{L_d}{d}\cdot exp\left(\frac{qVgas}{2*k_BT}\right)}} \quad (3)$$

where: L_d is the Debye length; d is the film thickness; g is the grain to grain contact; qV_{air} is the initial band bending in air; qV_{gas} is the band bending upon NO_2 exposure; k_BT is the thermal energy at 125°C (0.034 eV).

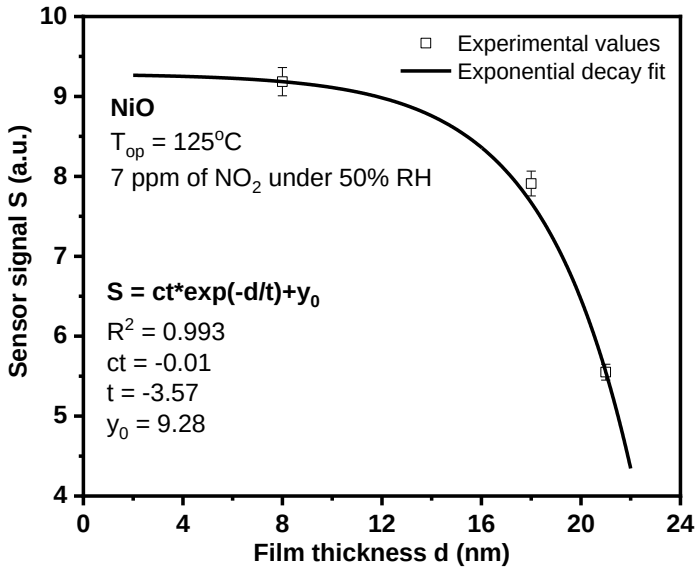

Fig. 12. Theoretical dependence of the sensor signal with respect to the layer thickness. The error bars represent the standard deviation between the experimental and the theoretical simulation

Considering the highest change in the band bending (sensor response under 7 ppm NO_2 exposure) and setting the initial band bending to the level of qV_{air} = 0.001 eV, and with an estimate of the grain-to-grain contact dimension of g=0.01 nm, we were able to identify how the thickness of the sensitive layer influences the gas sensing performance towards NO_2 detection for NiO sensors operated at 125°C under 50% RH (measured at 25°C). Consequently, based on the numerical approach one can clearly see that thin film NiO sensors exhibit sensor signal saturation towards NO_2 with decreasing film thickness. This effect is limited due to the contribution of the non-sensitive components such as grain-to-grain and metal-semiconductor contacts [14].

To complete an evaluation of the sensing properties of the NiO ultra-thin films, the sensitivity (selectivity) towards different analytes (CO, CH_4, NH_3 and SO_2) was acquired under the same operating conditions (Figure 13), by injecting each gas in turn (30 second dose time followed by 1 hour recovery time) after exposure to NO_2.

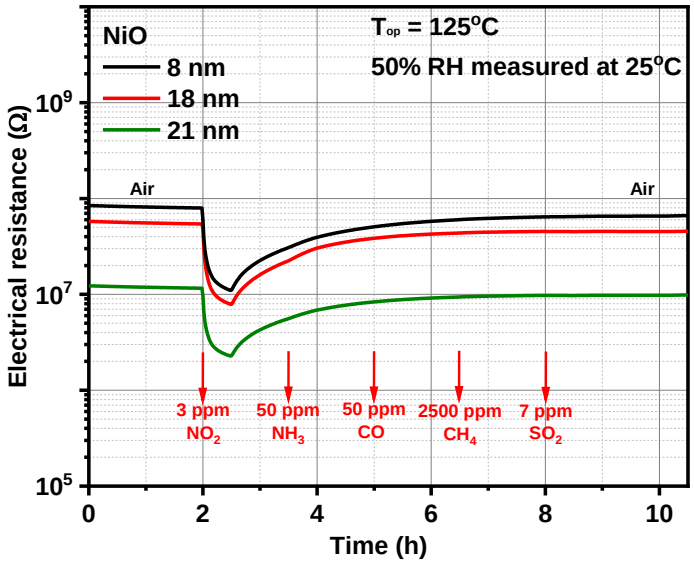

Fig. 13. Electrical resistance changes of the NiO sensors towards different target gases, under 50% RH at 125°C

The recovery time after exposure to NO_2 was clearly very long for these sensors (on the order of hours), leading to subsequent gas exposures taking place before the sensors had fully recovered. These long recovery times to NO_2 are commonly observed in sensors based on NiO (Supplementary Information); upon NO_2 exposure electrons from the valence band are thought to be trapped at the surface forming NO_2^- species, increasing hole concentration near the surface according to:

$$NO_2 + e^- \rightarrow NO_2^- + h^+$$

Since the majority charge carriers are holes this leads to a significant enhancement of the electrical conductivity of the NiO sensors (Figure 13). The electron affinity of NO_2 is around 2.3 eV whereas for molecular oxygen species the value is around only 0.4 eV [30] and therefore on removal of NO_2 the recovery transients might be expected to be longer than the response due to this difference in electron affinity between the two competing species on the same surface sites [31]. However subsequent exposure to the reducing gases used in this test would still be expected to display a noticeable change in resistance in the opposite direction to that found for NO_2 if a response was present. Previously, NiO thin films between 100 and 150 nm thick have been found to have some sensitivity towards NH_3 but only at temperatures above 275 °C [29] and NiO foils were found to

be less sensitive to toluene, formaldehyde, dichloromethane, chloroform, ethylacetate, isopropanol and heptane than to ammonia when tested at room temperature [21]. Our results indicate no measurable change in baseline resistance was detected when the ultrathin NiO films were exposed to NH_3, CO, CH_4 or SO_2 at the optimum sensing conditions for NO_2 (125°C).

In order to examine the reproducibility of the electrical resistance behavior, the sensors have been exposed, in a staircase evolution, to different NO_2 concentrations (0.8, 1, 3, 5 and 7 ppm) under 50% RH. The sensors showed good reproducibility after two cyclic measurements (Figure 14 and Table 1).

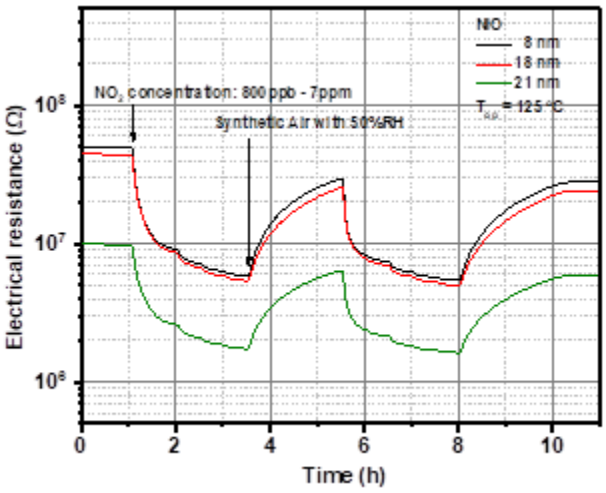

Fig. 14. Electrical resistance changes of different thickness NiO sensors towards various concentrations of NO_2, under 50% RH at 125°C

NO_2 conc.	Average resistance (Ohms)			Standard deviation		
ppm	8 nm	18 nm	21 nm	8 nm	18 nm	21 nm
0.8	$9.80*10^6$	$9.43*10^6$	$2.79*10^6$	$2.03*10^6$	$2.07*10^6$	$0.55*10^6$
1	$8.28*10^6$	$7.77*10^6$	$2.37*10^6$	$1.20*10^6$	$1.16*10^6$	$0.32*10^6$
3	$6.69*10^6$	$6.23*10^6$	$1.95*10^6$	$0.63*10^6$	$0.62*10^6$	$0.17*10^6$
5	$6.03*10^6$	$5.57*10^6$	$1.78*10^6$	$0.40*10^6$	$0.40*10^6$	$0.11*10^6$
7	$5.66*10^6$	$5.19*10^6$	$1.68*10^6$	$0.25*10^6$	$0.26*10^6$	$0.70*10^4$

Table 1: Electrical resistance changes of different thickness NiO sensors towards various concentrations of NO_2, under 50% RH at 125°C

Conclusions

NiO thin films have been deposited by CVD of [$Ni(dmamp)_2$] at substrate temperatures in the range of 250 – 400°C. For NiO films deposited at 300°C, the film thickness increased approximately linearly with deposition times above 5 hours. AFM and XRD analysis suggest that the film density and crystallinity increased with film thickness. XPS analysis confirmed the presence of Ni^{2+} on the film surfaces with $2p_{3/2}$ and $2p_{1/2}$ peak binding energies consistent with those reported in the literature. Ultra-thin (8 to 21 nm) NiO sensors were exposed to different RH levels over a wide range of operating temperatures in order to understand the influence of humidity and the NO_2 sensing properties, indicating the sensors were tolerant to humidity with an optimum sensing performance towards NO_2 for films deposited at 300 °C and operated at 125 °C. Moreover, we could derive a conduction model (e.g. identifying the energy of the initial band bending) based on potential changes and power law dependences of the subsequent sensor signal data. Thus, we could explain the humidity tolerance of the NiO sensors in the light of the low initial band bending value sustained by the essentially flat activation energy evolution with respect to different RH levels. The transduction model based on this numerical approach suggests that the ultra-thin film NiO sensors exhibit a strong interaction with NO_2, and selective sensitivity towards NO_2 was confirmed by exposure to different reducing gases.

Acknowledgments: This work was supported by the Engineering and Physical Sciences Research Council [grant number EP/M506448/1] and the Romanian National Authority for Scientific Research for funding through the Core Program PN 19-03 (contract no. 21N/2019) and project 12 PFE/2018. The authors would like to thank the University of Warwick for providing the alumina sensors and Alphasense Ltd for packaging the sensors.

References

[1] H. Ji, W. Zeng, Y. Li, Gas sensing mechanisms of metal oxide semiconductors: a focus review, Nanoscale 11 (2019) 22664.

[2] H. J. Kim, J. H. Lee, Highly sensitive and selective gas sensors using p-type oxide semiconductors: Overview, Sens. Actuators B Chemical 192 (2014) 607-627.
[3] T. P. Mokoena, H. C. Swart, D. E. Motaung, A review on recent progress of p-type nickel oxide based gas sensors: Future perspectives, Journal of Alloys and Compounds 805 (2019) 267-294.
[4] H. Nazemi, A. Joseph, J. Park, A. Emadi, Advanced Micro- and Nano-Gas Sensor Technology: A Review, Sensors 19(6) (2019) 1285.
[5] J. F. McAleer, P. T. Moseley, J. O. W. Norris, D. E. Williams, Tin dioxide gas sensors. Part 1. – Aspects of the surface chemistry revealed by electrical conductance variations, J. Chem. Soc. Faraday Trans. 83 (1987) 1323-1346.
[6] V. Sushmitha, V. Maragatham, P. Deepak Raj, M. Sridharan, Structural, electrical, optical and magnetic properties of NiO/ZnO thin films, IOP Conf. Series: Materials Science and Engineering 310 (2018) 012022.
[7] H. B. Charman, R. M. Dell, S. S. Teale, Chemisorption on metal oxides. Part1.- Nickel oxide, Transactions of the Faraday Society 59 (1963) 453-469.
[8] C. Drouet, P. Alphonse, J. L. G. Fierro, A. Rousset, Adsorption of nitric oxide and temperature programmed desorption on nonstoichiometric nickel-copper manganites, Applied Surface Science 174 (2001) 289-295.
[9] N. Barsan, D. Koziej, U. Weimar, Metal oxide based gas sensor research: how to? Sens. Actuators B Chemical 121 (2007) 18-35.
[10] I. Hotovy, V. Rehacek, P. Siciliano, S. Capone, Sensing characteristics of NiO thin films as NO_2 gas sensors, Thin Solid Films 417 (2002) 9-15.
[11] V. Patil, S. Pawar, M. A. Chougule, S. Patil, Development of NO_2 sensors using nickel oxide, Sensors and Transducers 131(8) (2011) 110-120.
[12] N. Yamazoe, K. Shimanoe, Roles of shape and size of component crystals in semiconductor gas sensors: I. Response to oxygen, Journal of Electrochemical Society 155(4) (2008) J85-J92.
[13] X. Du, S. M. George, Thickness dependence of sensor response for CO gas sensing by tin oxide films grown using atomic layer deposition. Sens. Actuators B Chemical 135 (2008) 152-160.
[14] R. L. Wilson, C. E. Simion, C. S. Blackman, C. J. Carmalt, A. Stanoiu, F. Di Maggio, J. A. Covington, The Effect of Film Thickness on the Gas Sensing Properties of Ultra-Thin TiO_2 Films Deposited by Atomic Layer Deposition, Sensors 18(3) (2018) 735.

[15] S. Pokhrel, C. E. Simion, V. Quemener, N. Barsan, U. Weimar, Investigations of conduction mechanism in Cr_2O_3 gas sensing thick films by ac impedance spectroscopy and work function changes measurements, Sens. Actuators B Chemical 133 (1) (2008) 78-83.
[16] N. Barsan, C. Simion, T. Heine, S. Pokhrel, U. Weimar, Modeling of sensing and transduction for p-type semiconducting metal oxide based gas sensors, Journal of Electroceramics 25 (2010) 11-19.
[17] Submitted.
[18] K.C Min, M. Kim, Y. H. You, S. S. Lee, Y. K. Lee, T. M. Chung, C. G. Kim, J. H. Hwang, K.-S. An, NiO thin films by MOCVD of $Ni(dmamb)_2$ and their resistance switching phenomena Surf. Coatings Technol., 201(22-23) (2007) 9252-9255.
[19] T. S. Yang, W. Cho, M. Kim, K.-S. An, T.-M. Chung, C. G. Kim, Y. Kim, Atomic layer deposition of nickel oxide films using $Ni(dmamb)_2$ and water, J. Vac. Sci. Technol. A, 23 (2005) 1238-1243.
[20] N. S. McIntyre, M. G. Cook, X-ray photoelectron studies on some oxides and hydroxides of cobalt, nickel, and copper, Anal. Chem., 47(13) (1975) 2208-2213.
[21] J. I. Langford, A. J. C. Wilson, Scherrer after sixty years: A survey and some new results in the determination of crystallite size, J. Appl. Crystallogr. 11(2) (1978) 102-113.
[22] J. Wang, P. Yang, X. Wei, High-Performance, Room-Temperature, and No-Humidity-Impact Ammonia Sensor Based on Heterogeneous Nickel Oxide and Zinc Oxide Nanocrystals, Applied Materials & Interface 7 (2015) 3816-3824.
[23] J. O. Guillen, S. Lany, A. Zunger, Nonstoichiometry and hole doping in NiO, AIP Conference Proceedings 128 (2010) 1199.
[24] S. Park, H-S. Ahn, C-K. Lee, H. Kim, Interaction and ordering of vacancy defects in NiO, Phys. Rev. B 77 (2008) 134103.
[25] I. Castro-Hurtado, C. Malagu, S. Morandi, N. Perez, G. G. Mandayo, E. Castano, Properties of NiO sputtered thin films and modeling of their sensing mechanism under formaldehyde atmospheres, Acta Materialia 61 (2013) 1146-1153.
[26] J. A. de Agapito, J. P. Santos, The interaction of low NO_2 concentrations in air with degenerate nanocrystalline tin dioxide thin films, Sens. Actuators B Chemical 31 (1996) 93-98.
[27] N. Yamazoe, K. Shimanoe, Theory of Power Laws for Semiconductor Gas Sensors, Sens. Actuators B Chemical 128 (2008) 566-573.

[28] N. Barsan, U. Weimar, Conduction Model of Metal Oxide Gas Sensors, Journal of Electroceramics 7 (2001) 143-167.

[29] I. Hotovy, J. Huran, L. Spiess, R. Capkovic, S. Hascik, Preparation and characterization of NiO thin films for gas sensor applications, Vacuum 58 (2000) 300-307.

[30] N. D. Hoa, N. Van Quy, D. Kim, Nanowire structured SnO_x-SWNT composites: High performance sensor for NO_x detection, Sens. Actuators B 142 (2009) 253-259.

[31] C. Cantalini, H.T. Sun, M. Faccio, M. Pelino, S. Santucci, L. Lozzi, M. Passacantando, NO_2 sensitivity of WO3 thin film obtained by high vacuum thermal evaporation, Sens. Actuators B 31 (1996) 81-87.

For TOC Only